

I Detect What I Don't Know: Incremental Anomaly Learning with Stochastic Weight Averaging-Gaussian for Oracle-Free Medical Imaging

Nand Kumar Yadav¹, Rodrigue Rizk¹, William C. W. Chen², and KC Santosh¹

¹ AI Research Lab, Department of Computer Science

² Biomedical & Translational Sciences, Sanford School of Medicine

University of South Dakota, Vermillion, SD 57069, USA

{nand.yadav, rodrigue.rizk, william.chen, kc.santosh}@usd.edu

Abstract. Unknown anomaly detection in medical imaging remains a fundamental challenge due to the scarcity of labeled anomalies and the high cost of expert supervision. We introduce an unsupervised, oracle-free framework that incrementally expands a trusted set of normal samples without any anomaly labels. Starting from a small, verified seed of normal images, our method alternates between lightweight adapter updates and uncertainty-gated sample admission. A frozen pretrained vision backbone is augmented with tiny convolutional adapters, ensuring rapid domain adaptation with negligible computational overhead. Extracted embeddings are stored in a compact coresnet enabling efficient k -nearest neighbor (k -NN) anomaly scoring. Safety during incremental expansion is enforced by dual probabilistic gates: a sample is admitted into the normal memory only if (i) its distance to the existing coresnet lies within a calibrated z -score threshold, and (ii) its SWAG-based epistemic uncertainty remains below a seed-calibrated bound. This mechanism prevents drift and false inclusions without relying on generative reconstruction or replay buffers. Empirically, our system steadily refines the notion of “normality” as unlabeled data arrive, producing substantial gains over baselines. On COVID-CXR, ROC-AUC improves from $0.9489 \rightarrow 0.9982$ (F1: $0.8048 \rightarrow 0.9746$); on Pneumonia-CXR, ROC-AUC rises from $0.6834 \rightarrow 0.8968$; and on Brain MRI ND-5, ROC-AUC increases from $0.6041 \rightarrow 0.7269$ and PR-AUC from $0.7539 \rightarrow 0.8211$. These results highlight the effectiveness and efficiency of the proposed framework for real-world, label-scarce medical imaging applications¹.

Keywords: Zero Anomaly Training, Incremental Learning, Stochastic Weight Averaging Gaussian (SWAG), Continual Learning, Bayesian Deep Learning

¹ Source code is publicly available at: <https://github.com/USD-AI-ResearchLab/Incremental-learning-Anomaly-Detection>

1 Introduction

Anomaly detection, the task of identifying data points that deviate significantly from the normal data distribution, is a fundamental problem across a range of applications, including fraud detection, medical diagnostics, and cybersecurity. The ability to detect anomalies is critical, as in medical imaging, particularly in early diagnosis tasks like COVID-19 screening or tumor identification. Traditionally, anomaly detection methods rely on labeled anomalous data, which allows a model to learn to differentiate between normal and anomalous instances. However, obtaining labeled anomalous data is often difficult, expensive, and sometimes impossible, particularly in domains where anomalies are rare or novel. This limitation motivates the need for unsupervised anomaly detection methods, which do not require anomalous samples for training.

Before deep learning models, anomaly detection relied largely on methods such as One-Class SVMs [1] and k -NN [2]. One-Class SVM, for instance, learns a decision boundary around the normal data, classifying anything outside this boundary as an anomaly. Similarly, k -NN identifies anomalies by measuring the distance between a data point and its nearest neighbors, flagging points as anomalous that are far from their neighbors. Classical methods work on low-dimensional data, but struggle with high-dimensional data (e.g., images) where distance metrics break down due to the curse of dimensionality. These methods are highly sensitive to hyperparameters (e.g., SVM kernels, the choice of k in k -NN) and often fail to capture complex relationships in image data, making them a poor fit for modern high-dimensional images.

To address these limitations, deep learning-based methods have gained traction in the field of anomaly detection. Autoencoders (AEs) and GANs [3] are now popular for anomaly detection in complex high-dimensional data. AEs learn a compact representation and try to reconstruct the input; samples with a large reconstruction error are treated as anomalies because they do not look “normal” to the model. Variants like VAEs [4] and denoising AEs [5] boost robustness and generalization, especially with noisy inputs. However, while AEs have shown success, they suffer from overfitting to the normal data distribution. This overfitting problem limits their practical use in detecting novel or rare anomalies. Furthermore, the performance of AEs heavily depends on the quality and quantity of normal data, and they may struggle to detect anomalies that deviate substantially from typical patterns in the normal dataset.

GANs [6] and AEs have been widely applied to anomaly detection. These models are typically trained on normal data with the goal of reconstructing or generating samples that resemble the normal distribution, such as AnoGAN [3]. Anomalies are then detected by identifying instances that the model reconstructs or generates poorly. However, such approaches suffer from several drawbacks. AEs often learn to reconstruct anomalies as well as normal data, leading to reduced discriminative power, while GANs are prone to training instability, sensitivity to hyperparameters, and require large amounts of normal data for effective training. These limitations hinder their scalability and robustness in real-world anomaly detection tasks.

More recently, representation-based methods such as PatchCore [7] have demonstrated superior performance by leveraging pretrained networks to extract patch-level embeddings of normal data. Instead of relying on generative reconstruction, PatchCore builds a memory bank of patch embeddings and detects anomalies by measuring the distances between test patches and their nearest neighbors in this memory. This avoids the pitfalls of generative approaches and enables robust, high-resolution anomaly localization.

Alongside these advances, incremental learning (IL) has emerged as a complementary strategy to reduce the reliance on large amounts of labeled anomalous data. By iteratively selecting the most informative or uncertain instances for labeling, IL improves model performance with minimal annotation effort. However, applying IL to anomaly detection remains challenging, as anomalies are rare or absent in training, making uncertainty estimation non-trivial.

To address these limitations, we propose a novel oracle-free, unsupervised anomaly detection framework that learns from a small initial set of normal samples and iteratively updates its normality model over time, entirely without requiring anomalous labels.

We build upon the PatchCore [8] architecture, known for its efficient, non-generative coresnet-based detection, and integrate it with: (a) incremental learning to update the memory bank with novel, high-confidence normal samples, (b) Stochastic Weight Averaging-Gaussian (SWAG) [9] to estimate epistemic uncertainty for gating sample inclusion. Our contributions are as follows:

- A novel IL-PatchCore+SWAG framework for unsupervised anomaly detection that incrementally expands the normal class distribution using adapter-based feature refinement and SWAG-driven uncertainty gating.
- A safe sample selection strategy combining distance-to-core and epistemic variance thresholds to prevent contamination of the normal memory bank.
- Demonstration of high detection performance on real-world datasets: COVID-CXR, Pneumonia Chest X-ray, and Brain MRI, outperforming strong baselines.

2 Related Works

2.1 Classical Anomaly Detection Methods

Classical anomaly detection techniques such as One-Class SVM [1] and k -NN [2] were among the earliest unsupervised approaches: the former encloses normal data within a decision boundary and flags points outside it, while the latter measures a sample’s distance to its nearest neighbors and treats large distances as anomalous. Despite their historical impact, these methods face well-known limitations. In high-dimensional settings, distance metrics become less discriminative, eroding the effectiveness of k -NN style detectors; One-Class SVM is notably sensitive to kernel and regularization choices, often demanding costly cross-validation; and both families struggle to model the complex, structured

dependencies present in images or sequences. Consequently, although they remain practical for simple, low-dimensional problems, their performance degrades on modern, high-dimensional data, motivating the shift toward deep learning-based methods that can better capture rich feature hierarchies.

2.2 Deep Learning-Based Anomaly Detection

Deep learning approaches, particularly AEs and GANs, have become widely adopted for anomaly detection in high-dimensional and complex domains such as image data.

AEs. AEs are neural networks that learn compressed latent representations of input data with the objective of reconstructing the original inputs. Anomaly scores are typically derived from reconstruction error, with higher errors indicating a greater likelihood of anomalousness. Variants such as VAEs [4] and Denoising AEs [5] have been proposed to improve reconstruction fidelity and generalization. Despite their popularity, AEs exhibit notable limitations. They are prone to reconstruction bias, often overfitting to normal data and thereby reducing their ability to generalize to unseen anomalies [10]. Furthermore, their effectiveness is strongly dependent on the availability of abundant, high-quality normal data, which limits their applicability in settings with scarce or imbalanced datasets.

Generative Adversarial Networks (GANs) and PatchCore. GANs, composed of a generator and discriminator pair, have also been investigated for anomaly detection. The generator aims to approximate the distribution of normal data, while the discriminator distinguishes between real and synthetic samples, with anomalies identified when they fall outside the modeled distribution [1]. Despite their potential, GAN-based approaches suffer from several limitations. They are prone to training instability and mode collapse, which can result in incomplete coverage of the normal distribution [6]. Moreover, training an effective GAN typically requires large volumes of normal data, which is often impractical in real-world anomaly detection scenarios. GANs are highly sensitive to hyperparameters, making them computationally expensive and difficult to optimize reliably. These drawbacks restrict their scalability and limit their robustness as a practical solution for anomaly detection. PatchCore [8] is a state-of-the-art approach for unsupervised anomaly detection that avoids the need for generative modeling. Instead of reconstructing or synthesizing images (as in AEs or GANs), PatchCore directly leverages deep features from pretrained convolutional networks. It extracts multi-scale patch-level features from training images and stores a compact subset in a memory bank using coresnet subsampling. This design has several advantages: it avoids the training instability of GANs, overgeneralization issues of AEs, and requires only normal data for building the memory bank.

Consequently, PatchCore achieves high detection accuracy with efficient inference, making it well-suited for industrial and medical anomaly detection tasks. However, PatchCore also suffers from large memory requirements during the

feature storage and learning phase, since even the coresets can grow significantly with data size. To address this drawback, we propose incorporating IL to select only the most informative samples from the pool. Additionally, we use SWAG-based uncertainty estimation to guide the selection of the most appropriate samples. This makes the method more computationally efficient, memory-friendly, and better suited for real-time deployment, while maintaining high detection performance.

IL in Anomaly Detection. Incremental (continual) learning updates a model as data arrive over time while avoiding catastrophic forgetting. In anomaly detection this is especially challenging: (i) the data distribution drifts (both covariate and semantic), so a static threshold or memory quickly becomes obsolete; (ii) anomalies are rare and diverse, so incremental updates risk *contaminating* the normal model when labels are absent; (iii) strict memory and latency budgets limit rehearsal of past data, exacerbating the stability–plasticity trade-off; and (iv) most continual-learning methods assume task or class labels and class-balanced streams, assumptions that rarely hold in one-class settings. Consequently, effective incremental anomaly detection requires drift-aware calibration, bounded exemplar memories (e.g., coresets selection), to preserve prior normality, ideally under weak or no anomaly labels [11,12,13,14]. This perspective aligns with our design: we update the detector online using a frozen normal memory with cautious admission criteria and lightweight adapter tuning, thereby maintaining past competence while adapting to new normal regimes without relying on labeled anomalies.

Anomaly Detection Without Anomalous Training Data. Recent methods remove the need for anomalous training labels by first modeling normality and then flagging deviations. Self-supervised one-class objectives and patch-based methods fall into this camp: they learn feature spaces where normal samples are compact and anomalies appear distant. Despite promising results, purely unsupervised pipelines remain vulnerable to pool contamination (i.e., inadvertent inclusion of anomalies), and they rarely provide a principled way to *expand* the normal manifold once deployment uncovers new, legitimate variability. These limitations motivate our approach. Starting from a small, trusted seed of normals, we enlarge the normal set incrementally. At each step, a candidate is admitted only when its PatchCore distance is statistically consistent with the seed distribution and its epistemic uncertainty estimated via SWAG is low. This dual evidence gate improves robustness to contamination and offers a principled path for safe, label-free growth of the memory bank, addressing both data efficiency and long-term stability of the detector.

3 Motivation

This work is motivated by the following question: *can we safely grow the set of normals without ever consulting an oracle?* Our answer is to use pool-based selection with IL under a *dual-evidence gate*. Concretely, we start from a small, trusted

seed of normals, build a compact PatchCore memory via coresnet subsampling [7], and then expand that memory only with pool samples that simultaneously (i) score low under PatchCore k -NN distance after seed-based z-normalization (statistical evidence), and (ii) exhibit low epistemic uncertainty under a SWAG posterior over the adapter [9] (Bayesian evidence). In contrast to traditional active learning [15], where high uncertainty triggers an expensive query, uncertainty here acts as a *filter*: items are admitted *only if* the model is confident they lie inside the current normal manifold. The adapter is then updated briefly on the admitted samples. This incremental active [16],[17] recipe is attractive for three reasons. First, it is *oracle-free and data-efficient*: a tiny seed bootstraps a detector that improves as new, confident normals arrive. Second, it is *robust*: the dual gate limits contamination from hidden anomalies, while seed-relative z-scores and periodic recalibration provide drift awareness. Third, it is *scalable*: PatchCore avoids generative training, and under mild separation/concentration assumptions, adding verified normals can only lower expected normal scores, so in the clean limit the normal manifold sharpens, giving a principled path to stable, label-free improvement over time.

In short, our motivation is practical and structural: replace an impractical human oracle with a Bayesian filter, couple it with a conservative statistical test relative to a trusted seed, and grow normality incrementally with bounded risk so anomaly detectors remain accurate, robust, and maintainable under real deployment constraints.

4 Proposed Method

We consider image anomaly detection where training images come primarily from a *normal* class, while the test set contains both normal and anomalous samples. We adopt a PatchCore-style non-parametric detector built on a frozen, pretrained ResNet backbone f_θ . Given an image $x \in [0, 1]^{C \times H \times W}$, multi-scale feature maps are extracted and passed through a lightweight adapter g_ϕ that projects each scale to a common width; the outputs are bilinearly aligned, with channel-concatenated, and ℓ_2 -normalized to yield per-location patch embeddings. A memory bank \mathcal{M} of normal embeddings is constructed from trusted seed data via farthest-first (coreset) selection. We incorporate SWAG-based uncertainty estimates to complement distance scoring. From an unlabeled pool, additional pseudo-normal samples are admitted only when statistical and epistemic evidence supports their inclusion, enabling a cautious but steady enlargement of the normal manifold. This setting highlights the fundamental difficulty of anomaly detection: while normal data are abundant and well-characterized, anomalies remain rare, diverse, and context dependent, making them unsuitable for a supervised approach. On the other hand, unsupervised learning from large data pools [18] risks contamination, since even a small fraction of anomalies can distort the learned statistics. Our formulation begins with a small, trusted seed of normal data and carefully grows outward, admitting new samples under principled uncertainty checks. This progressive, evidence-driven expansion

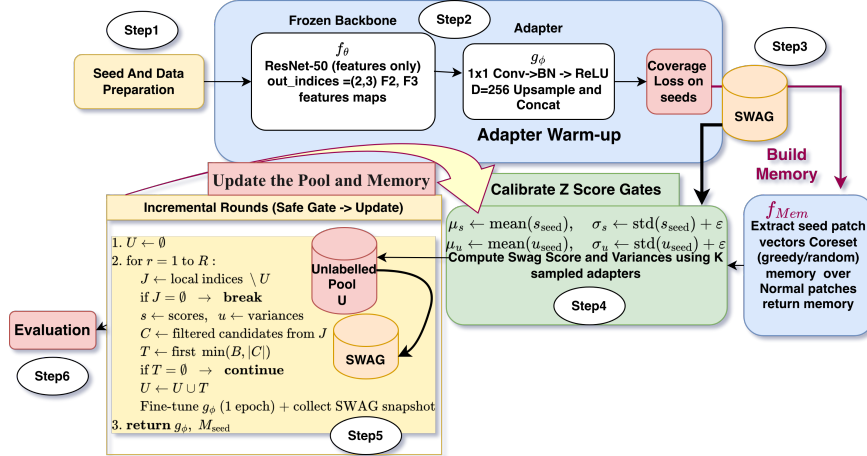


Fig. 1: Pipeline of the proposed anomaly-detection framework.

of normality ensures robustness, efficiency, and stability, and sets the stage for our algorithms (Algos. 1–6) that formalize each component of this process. The overall pipeline is depicted in Fig. 1.

Our method operates over iterative rounds. Each round: (1) scores incoming unlabeled data using PatchCore-based k -NN anomaly scoring, (2) uses SWAG to estimate uncertainty on these samples, (3) selects high-confidence normal candidates based on: distance thresholding to the coresset, and epistemic uncertainty z-score relative to seed distribution, (4) admits selected samples into the coresset memory, and (5) updates the adapter modules (only) to improve representations. The process begins with a seed set of trusted normal samples as illustrated in Algo. 1. Furthermore, we use an adapter for learning the normal samples, as shown in Algorithm 2. Simultaneously, we populate a prototype memory by coresset selection from the seed embeddings as illustrated in Algo. 3. This memory serves as a compact summary of the normal distribution, a reference structure against which all future candidates can be evaluated. Crucially, in our implementation, this seed memory remains fixed for the entirety of training, providing a stable foundation that prevents contamination by the pool. Even if a sample looks close to what we’ve seen before, the model also has to admit what it doesn’t know. A point might sit near our “normal” prototypes, but if the model is highly uncertain about its representation, admitting it could be risky. To address this, we equip the adapter with a Bayesian posterior approximation using SWAG, which maintains a distribution over its weights. By sampling multiple parameter realizations and scoring each candidate, we estimate both the mean distance $\mu(x)$ and variance $v(x)$ as illustrated in Algo. 4. The mean captures how closely a sample resembles normal patterns, while the variance captures epistemic uncertainty: how consistently the model agrees on this assessment.

Algorithm 1 (Step 1): Seed & Data Preparation

Inputs: Normal dir dir_0 , Anomaly dir dir_1 , image size S , color $\in \{\text{L}, \text{RGB}\}$

- 1: $\mathcal{X} \leftarrow$ load all images from $\text{dir}_0, \text{dir}_1$; resize to (S, S) ; scale to $[0, 1]$
- 2: Label mapping: $\text{NORMAL} \mapsto 0, \text{ANOMALY} \mapsto 1$
- 3: $\mathcal{I}_0 \leftarrow \{i : y_i = 0\}$ ▷ all normals
- 4: Shuffle \mathcal{I}_0 ; $n \leftarrow \max(1, \lfloor 0.30 \cdot |\mathcal{I}_0| \rfloor)$
- 5: $\mathcal{I}_{\text{seed}} \leftarrow$ first n of \mathcal{I}_0 ; $\mathcal{I}_{\text{rest}} \leftarrow \mathcal{I}_0 \setminus \mathcal{I}_{\text{seed}}$
- 6: $\mathcal{I}_{\text{anom}} \leftarrow \{i : y_i = 1\}$; $\mathcal{I}_{\text{pool}} \leftarrow \mathcal{I}_{\text{rest}} \cup \mathcal{I}_{\text{anom}}$
- 7: **return** $(\mathcal{X}, \mathcal{I}_{\text{seed}}, \mathcal{I}_{\text{pool}})$

The central decision is then governed by a *z-score gate*. For each candidate, we normalize its score and uncertainty relative to the seed distribution:

$$z_s(x) = \frac{\mu(x) - \mu_s}{\sigma_s}, \quad z_u(x) = \frac{v(x) - \mu_u}{\sigma_u}. \quad (1)$$

The sample is qualified as a pseudo-normal only when $z_s(x)$ and $z_u(x)$ are at most 1.0. If no candidates pass, the gates may be relaxed once to 1.5σ . Unlike earlier designs, there is no borderline band or fusion ranking: acceptance is a strict intersection of score and uncertainty gates. This mechanism enforces selective trust, ensuring that only statistically safe samples are admitted. Accepted samples are then used for a brief adapter update, typically a single compact epoch, and the new weights are snapshotted into the SWAG ensemble. This incremental tuning allows the adapter to expand its coverage of P_N without ever altering the frozen seed memory. The process repeats for several rounds until the pool is exhausted or no new candidates are admitted. In this way, the system grows cautiously: expanding its representation of normality while keeping the calibration anchored to the uncontaminated seed, the procedure is illustrated in Algo. 5.

Finally, evaluation is straightforward as illustrated in Algo. 6. A test image is scored by PatchCore distances to the seed memory, using the most up-to-date adapter and SWAG ensemble. Anomalies emerge as those samples whose scores or uncertainties exceed the calibrated bounds. Each component plays a precise role: the seed set prevents initial contamination; the adapter tailors the latent space to the domain; SWAG quantifies epistemic uncertainty; the dual z-score gates prevent unsafe admissions; and the iterative loop allows gradual, self-supervised growth. What emerges is a robust, oracle-free learner: a model that begins with modest seeds, acknowledges its own uncertainty, and safely expands its knowledge of normality through IL.

Implications. Let

$$\beta = \Pr_{x \sim P_N} (z_s(x) \leq \tau_z \wedge z_u(x) \leq \tau_z)$$

denote the acceptance probability of the dual gate for *true normal* samples, with an optional one-time relaxation $\tau_z : 1.0 \rightarrow 1.5$ if required. In the `strict_normal_only =True`, configuration (i.e., oracle-assisted mode), only gate-passing items whose ground-truth label is $y=0$ are used to update the adapter g_ϕ and to expand the

Algorithm 2 (Step 2): Initialize Model and Warm-Up Adapter

Inputs: Frozen backbone f_θ , adapter g_ϕ (per-scale 1×1 Conv+BN+ReLU, dim $D=256$), seed indices $\mathcal{I}_{\text{seed}}$, epochs E , lr η , prototype budget K
Outputs: Warmed g_ϕ and initialized SWAG

- 1: Set f_θ to eval; initialize g_ϕ
- 2: Build seed vectors V_{seed} (**no per-image cap, native grid**):
 - for $x \in \mathcal{I}_{\text{seed}}$: get multi-scale $\{F_\ell\}$; project $A_\ell = g_\phi^\ell(F_\ell)$; upsample each A_ℓ to the **common native size** $(H_{\text{max}}, W_{\text{max}})$ of that image; concatenate channel-wise to A ; flatten and ℓ_2 -normalize to get Q ; append all Q to V_{seed} .
- 3: $\rho \leftarrow \min(1, K/|V_{\text{seed}}|)$; $P \leftarrow \text{CORESETGREEDY}(V_{\text{seed}}, \rho)$
- 4: **for** $e = 1..E$ **do** ▷ backbone frozen
- 5: **for** minibatches of $x \in \mathcal{I}_{\text{seed}}$ **do**
- 6: Extract Q as above; $\mathcal{L} \leftarrow \frac{1}{|Q|} \sum_i \min_{\mathbf{p} \in P} \|\mathbf{q}_i - \mathbf{p}\|_2$
- 7: Update g_ϕ with Adam(lr= η) on \mathcal{L}
- 8: **end for**
- 9: **end for**
- 10: Initialize SWAG on g_ϕ and take **two** snapshots
- 11: **return** warmed g_ϕ , SWAG state

Algorithm 3 (Step 3): Build Initial Normal Memory (PatchCore)

Inputs: f_θ , warmed g_ϕ , seed set $\mathcal{I}_{\text{seed}}$, coresnet ratio ρ_m , grid 16×16 , cap τ
Outputs: Initial memory \mathcal{M}_0

- 1: Extract V_{seed} as in Alg. 2; $\mathcal{M}_0 \leftarrow \text{CORESETGREEDY}(V_{\text{seed}}, \rho_m)$
- 2: **return** \mathcal{M}_0 ▷ Note: in incremental rounds we *grow/rebuild* memory with accepted normals

PatchCore memory \mathcal{M} . Each admitted batch therefore contributes $\Theta(\beta)$ genuine normal samples, incurs *zero* anomaly contamination, and follows the standard finite-sample error decay $O(1/\sqrt{m})$ as the memory size m increases. The dual gate serves as a conservative prefilter, requiring both low normalized distance (z_s) and low uncertainty (z_u), thereby improving sample efficiency while maintaining safety. Uncertainty is ignored only in degenerate cases where σ_u is numerically negligible.

Theorem 1 (Oracle-assisted zero-contamination under dual-gate prefilter).

Assume an oracle-assisted variant of Alg. 5, implemented conceptually via `strict_normal_only =True`. After the dual gate (z_s, z_u) selects candidates satisfying $z_s(x) \leq \tau_z$ and $z_u(x) \leq \tau_z$, the ground-truth label $y(x)$ is queried, and only samples with $y=0$ are admitted for

Algorithm 4 (Step 4): Calibrate Z-Score Gates (on seeds)

Inputs: f_θ , g_ϕ , memory \mathcal{M}_0 , seed set $\mathcal{I}_{\text{seed}}$, k -NN $k=3$, top- q (e.g. 0.03 – 0.05), SWAG samples K
Outputs: $(\mu_s, \sigma_s, \mu_u, \sigma_u)$ and flag `useU`

- 1: For each $x \in \mathcal{I}_{\text{seed}}$: compute $s(x)$ via PatchCore top- q rule with \mathcal{M}_0
- 2: For each $x \in \mathcal{I}_{\text{seed}}$: sample K SWAG adapters, get $u(x) = \text{Var}[s^{(k)}(x)]$
- 3: $\mu_s, \sigma_s \leftarrow \text{mean}/\text{std}(\{s(x)\})$; $\mu_u, \sigma_u \leftarrow \text{mean}/\text{std}(\{u(x)\})$
- 4: $\text{useU} \leftarrow (\sigma_u > 10^{-6})$ ▷ if SWAG variance is numerically non-zero
- 5: **return** $(\mu_s, \sigma_s, \mu_u, \sigma_u, \text{useU})$

Algorithm 5 (Step 5): Incremental Rounds (Growing Memory + Gated Ranking + Checkpointing)

Inputs: Backbone f_θ (frozen), adapter g_ϕ , SWAG state; pool $\mathcal{I}_{\text{pool}}$; rounds R ; budget B ; calibration $(\mu_s, \sigma_s, \mu_u, \sigma_u, \text{useU})$; thresholds $\tau_z = 1.0 \rightarrow 1.5$ (one relaxation); ranking mode $\in \{\text{boundary, uncert}\}$; strict-normal-only flag (False/True); resume policy $\in \{\text{best_so_far, last}\}$.

Outputs: Final adapter g_ϕ^* and memory \mathcal{M}^* .

```

1:  $\mathcal{U} \leftarrow \emptyset$             $\triangleright$  used local pool indices;    $\mathcal{A} \leftarrow \emptyset$             $\triangleright$  accepted normal indices
2: Save best_overall checkpoint of  $g_\phi$  using a metric (validation AUC if available, else
    $\bar{s}_{\text{pool}} - \bar{s}_{\text{seed}}$  on a fixed subset)
3: for  $r = 1$  to  $R$  do
4:   Resume  $g_\phi$  from best_overall (or last) per policy
5:   Build memory from seeds  $\cup$  accepted normals:  $\mathcal{M}_r \leftarrow \text{CORESETGREEDY}(V(\mathcal{I}_{\text{seed}} \cup$ 
    $\mathcal{A}), \rho_m)$ 
6:    $\mathcal{J} \leftarrow \{0, \dots, |\mathcal{I}_{\text{pool}}| - 1\} \setminus \mathcal{U}$ ;
7:   if  $\mathcal{J} = \emptyset$  then break
8:   end if
9:   Score pool with  $\mathcal{M}_r: \{s_j\}_{j \in \mathcal{J}}$ ; if useU then also  $\{u_j\}_{j \in \mathcal{J}}$  else  $u_j \leftarrow 0$ 
10:  Normalize:  $z_j^s = (s_j - \mu_s) / \sigma_s$ ;  $z_j^u = (u_j - \mu_u) / \sigma_u$ 
11:  Safe set:  $\mathcal{C} \leftarrow \{j \in \mathcal{J} \mid z_j^s \leq \tau_z \wedge (\neg \text{useU} \vee z_j^u \leq \tau_z)\}$ 
12:  if  $\mathcal{C} = \emptyset$  then set  $\tau_z \leftarrow 1.5$  and recompute  $\mathcal{C}$ ;
13:  if  $\mathcal{C} = \emptyset$  then continue
14:  end if
15:  end if
16:  Rank in  $\mathcal{C}$ :
   boundary: sort by  $s_j$  (desc);  uncert: sort by  $z_j^u$  (desc)
17:   $\mathcal{T} \leftarrow \text{top-min}(B, |\mathcal{C}|)$  locals after ranking
18:  Mark used:  $\mathcal{U} \leftarrow \mathcal{U} \cup \mathcal{T}$ ;  map to globals  $\mathcal{G} \leftarrow \{\mathcal{I}_{\text{pool}}[j] \mid j \in \mathcal{T}\}$ 
19:  if strict-normal-only then
20:    Filter true normals:  $\mathcal{G} \leftarrow \{g \in \mathcal{G} \mid y_g = 0\}$ 
21:    if  $|\mathcal{G}| = 0$  then
22:      Save last; continue
23:    end if
24:  else
25:    // Unsupervised mode (no labels used from the pool)
26:    Treat all selected samples as presumed normals:  $\mathcal{G} \leftarrow \mathcal{T}$ 
27:  end if
28:  Fine-tune  $g_\phi$  for 1 epoch on  $\mathcal{G}$  with prototype loss (backbone frozen); take a
   SWAG snapshot
29:  Grow memory:  $\mathcal{A} \leftarrow \mathcal{A} \cup \mathcal{G}$ 
30:  Checkpoint: save last; recompute metric; if improved, update best_overall
31: end for
32: Restore  $g_\phi^*$  from best_overall;  build  $\mathcal{M}^* \leftarrow V(\mathcal{I}_{\text{seed}} \cup \mathcal{A})$ 
33: return  $g_\phi^*, \mathcal{M}^*$ 

```

Algorithm 6 (Step 6): Evaluate on Held-out Test

Inputs: Test loader $\mathcal{D}_{\text{test}}$, $f_\theta, g_\phi, \mathcal{M}$, labels $\{y_i\}$

- 1: Compute image-level anomaly scores $\{s_i\}$ via PatchCore (top- q of k -NN distances to \mathcal{M})
- 2: **if** $\{y_i\}$ contains both classes **then**
- 3: Build ROC; $\text{AUC} \leftarrow$ area under ROC
- 4: $t^* \leftarrow \arg \max_t (\text{TPR}(t) - \text{FPR}(t))$ ▷ Youden's J
- 5: $\hat{y}_i \leftarrow \mathbb{1}[s_i \geq t^*]$; report ACC, Precision, Recall, F1
- 6: (Optional) save ROC/PR plots and example heatmaps
- 7: **else**
- 8: Skip thresholded metrics (no positives/negatives)
- 9: **end if**

adapter updates and memory expansion. Then the contamination rate of the memory bank,

$$\alpha = \Pr[x \in \mathcal{M} \wedge y(x)=1],$$

is identically $\alpha = 0$ for all active-learning rounds, independent of the gate threshold relaxation and SWAG sampling settings.

Proof sketch. By construction, the oracle-assisted update rule admits only samples with $y=0$. Hence $\Pr[x \in \mathcal{M} \wedge y(x)=1] = 0$ for all rounds. The dual gate (z_s, z_u) merely determines which items are *considered*; the oracle filter decides which are actually *added*.

Proposition 1 (Oracle-free dual-gate bound (image level)). *If the oracle filter is disabled (`strict_normal_only=False`) and there exist separation margins $\gamma_s, \gamma_u > 0$ such that for all anomalous $x \sim P_A$ either $z_s(x) \geq 1 + \gamma_s$ or $z_u(x) \geq 1 + \gamma_u$, then, with K SWAG samples and unbiased, finite-variance estimators of $d(x)$ and $u(x)$, the probability that an anomaly passes the dual gate $z_s(x) \leq 1$ and $z_u(x) \leq 1$ satisfies*

$$\Pr_{x \sim P_A} [\text{admit}(x)] \leq \delta + \exp\left(-cK \cdot \min\left\{\frac{\gamma_s^2}{\sigma_s^2}, \frac{\gamma_u^2}{\sigma_u^2}\right\}\right),$$

for some universal constant $c > 0$, where δ accounts for finite-sample concentration. In degenerate cases where $\sigma_u \approx 0$, the decision reduces to the single-score gate on z_s alone.

Incremental Learning with and without an Oracle. Classical IL forwards uncertain samples to an oracle [19]. The uncertainty acts as a filter: only low-distance, low-uncertainty candidates are eligible. With the oracle filter (our default), memory growth is provably contamination-free (Thm. 1); without it, the dual gate provides the probabilistic safety in Prop. 1.

5 Experimental Setup, Results, and Discussion

The experimental setup uses a frozen ResNet-50 backbone with selected scales projected by an adapter using 1×1 Conv+BN+ReLU layers to a width of 256, normalized channel-wise before patch flattening. During warm-up, prototypes

are formed on seed normals at native resolution with a prototype-coverage loss, and SWAG is initialized with adapter snapshots. For memory, compact 16×16 patch grids are used for images, while scoring uses full-resolution aligned maps. SWAG generates sampled adapters by perturbing floating weights, and dual gating with z-scores on PatchCore scores and variance filters candidates, with relaxed thresholds if necessary. Selection ranks safe items either by boundary score or uncertainty, then adapters are fine-tuned strictly on accepted normals with small updates, followed by new SWAG snapshots and memory rebuilds. A best-so-far checkpoint is maintained based on validation AUC. Scoring employs PatchCore with $k = 3$ and top-3-5% patch fraction, and performance is reported with ROC-AUC, PR-AUC, and thresholds like Youden's J [20] or target precision.

Hyperparameter Settings. All experiments were implemented using random seeds (123–127) to ensure reproducibility. The learning rate was set to 1×10^{-4} during initial adapter training and reduced to 3×10^{-5} for incremental fine-tuning, providing stable convergence while preserving previously learned representations. We used a batch size of 32, a coresset memory ratio of 0.3, and performed five active learning rounds with a budget of 200 samples per round for the Chest-xray dataset and 500 for the Brain MRI dataset. The SWAG uncertainty estimation was configured with a noise scale of 0.02 and $K=4$ model samples. For PatchCore scoring, we used a top- $q=0.03$ percentile and $k=3$ nearest neighbors. The gating threshold τ_z was dynamically relaxed from 1.0 to 1.5 when no safe candidates were found in the uncertainty-aware selection step. All hyperparameters were empirically chosen to balance computational efficiency, convergence stability, and robustness across datasets.

5.1 Datasets

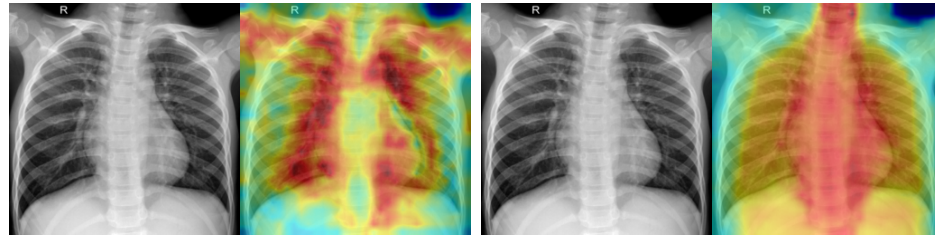
We evaluate the proposed framework on three medical imaging datasets:

- *Chest X-Ray (Pneumonia) Dataset.* We used publicly available *Chest_xray (Pneumonia)* [21] dataset which comprises 1,341 normal and 3,875 pneumonia Chest radiographs. For our experiments, we constructed a stratified evaluation subset of 624 images with 234 normal and 390 pneumonia cases and the rest as a training subset.
- *COVID-CXR Dataset.* The COVID Chest X-ray dataset [22]. The training set comprises 460 COVID-positive cases [23] and 1,266 normal samples, and the test set includes 116 COVID-positive and 317 normal samples.
- *Brain MRI ND-5.* The Brain MRI ND-5 dataset [24]³ includes a training split with 8,389 abnormal images (excluding duplicate files as .png) and 2,339 normal images, and a test split of 2,806 axial slices (1,975 tumor, 831 normal).

³ <https://ieee-dataport.org/documents/brain-mri-nd-5-dataset>

Table 1: Comparison at the Youden-optimal threshold across datasets.

Dataset	Setting	ROC	AUC	PR	AUC	Thr* (Youden)	ACC	Precision	Recall	F1	TN	FP	FN	TP
<i>Chest_xray (Pneumonia)</i>	Baseline (PatchCore)	0.6834	0.7656	0.993364	0.6538	0.7620	0.6487	0.7008	155	79	137	253		
	Baseline + Adapter warmup	0.8820	0.9267	0.952984	0.7628	0.9060	0.6923	0.7849	199	35	97	293		
	Proposed (Post-IL, Oracle-free)	0.8968	0.9372	0.953104	0.8093	0.8796	0.8051	0.8407	191	43	76	314		
<i>COVID-CXR</i>	Baseline (PatchCore)	0.9489	0.8976	0.989044	0.8868	0.7481	0.8707	0.8048	283	34	15	101		
	Baseline + Adapter warmup	0.9961	0.9898	0.954467	0.9792	0.9652	0.9569	0.9610	313	4	5	111		
	Proposed Method	0.9982	0.9951	0.953187	0.9861	0.9583	0.9914	0.9746	312	5	1	115		
<i>Brain MRI ND-5</i>	Baseline (PatchCore)	0.6041	0.7539	0.961838	0.6216	0.7695	0.6608	0.7109	440	391	671	1304		
	Baseline + Adapter warmup	0.6632	0.8174	0.966118	0.7327	0.8083	0.8132	0.8107	450	381	369	1606		
	Proposed Method	0.7269	0.8211	0.970559	0.7445	0.8086	0.8344	0.8213	441	390	327	1648		

Fig. 2: Corresponding heatmaps for baseline (left) and proposed IL approach (right) on *Chest_xray* dataset.

5.2 Results Analysis

a) *Chest X-Ray (Pneumonia) Dataset*. We compare a baseline PatchCore system (memory from the full training set, no IL) against our proposed IL strategy using the Chest X-Ray dataset, which begins with 30% seed normal samples. Evaluation is performed on a held-out test set with mixed labels. As shown in Table 1, IL substantially improves performance across multiple metrics. ROC-AUC increases from 0.6834 (baseline) to 0.8968, while PR-AUC improves from 0.7656 to 0.9372. Accuracy also rises from 0.6538 to 0.8093. Precision improves from 0.7620 to 0.8796, with recall increasing from 0.6487 to 0.8051, resulting in an F1 gain from 0.7008 to 0.8407. In addition to these improvements, false positives are reduced from 79 to 43 while true positives increase from 253 to 314. Fig. 2 illustrates the heatmap of the baseline and proposed method, which shows the proposed method focusing better on the important regions. We depicted the baseline and proposed methods' PR and ROC curves in Fig. 3. For a clearer illustration of the number of correctly predicted samples compared to baseline, we present the confusion matrices in Fig. 4.

b) *COVIDCXR Dataset*. Table 1 reports results on the COVID Chest X-ray dataset. Our incremental learning approach delivers substantial improvements over the baseline. ROC AUC improves from 0.9489 to 0.9982, and PR AUC rises from 0.8976 to 0.9951. At the Youden-optimal threshold, accuracy increases from 0.8868 to 0.9861. Precision improves from 0.7481 to 0.9583, recall from 0.8707 to 0.9914, and F1 score from 0.8048 to 0.9746. In terms of confusion matrix entries, true negatives increase (283 → 312), false positives decrease (34 → 5), false negatives are reduced (15 → 1), and true positives rise (101 → 115). IL not only

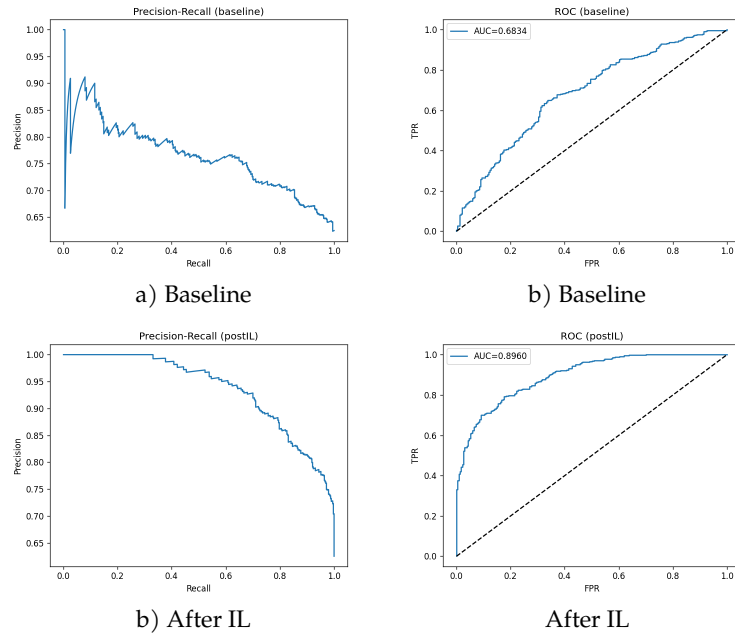


Fig. 3: PR and ROC curves before and after IL on the Chest_xray dataset.

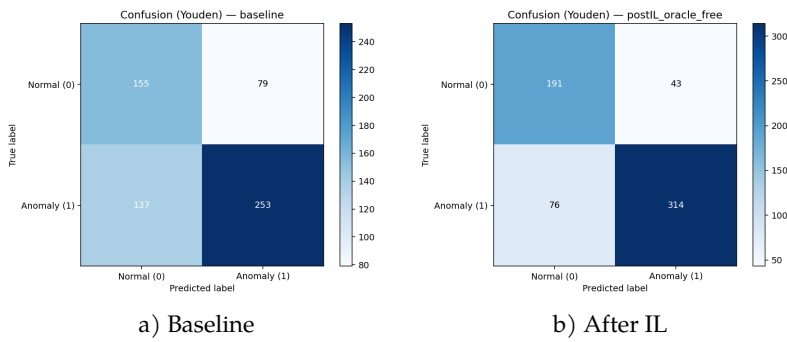


Fig. 4: Confusion matrices before and after IL. IL improves performance.

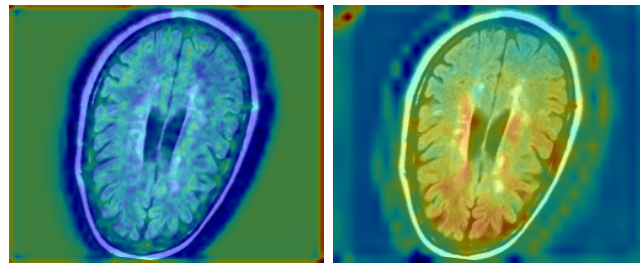


Fig. 5: Brain MRI dataset representative heatmaps before (left) and after IL (right).

Table 2: Comparison of uncertainty estimation strategies across oracle and oracle-free settings on Chest_xray.

Setting	Uncertainty	ROC AUC	PR AUC	ACC	Precision	F1
Oracle-Free	None	0.8685	0.8934	0.7841	0.8705	0.7692
Oracle-Free	SWAG	0.8968	0.9372	0.8093	0.8796	0.8407
Oracle-Free	MC Dropout	0.8438	0.8797	0.7710	0.8601	0.7692
Oracle-Free	Ensemble	0.8828	0.9021	0.8060	0.8800	0.8380
Oracle-Based	None	0.8372	0.8733	0.7683	0.8642	0.7561
Oracle-Based	SWAG	0.8960	0.9366	0.8045	0.8829	0.8351
Oracle-Based	MC Dropout	0.8099	0.8608	0.7604	0.8534	0.7521
Oracle-Based	Ensemble	0.8594	0.8893	0.7950	0.8790	0.8320

improves ROC-AUC and PR-AUC but also reduces false positives (from 34 to 5) while increasing true positives (from 101 to 115).

c) *Brain MRI Dataset (ND-5)*: We evaluated our approach on the Brain MRI ND-5, compared with the baseline we used 500, the proposed method improves all metrics: ROC-AUC rises from 0.6041 to **0.7269** and PR-AUC from 0.7539 to **0.8211**. At the Youden-optimal threshold (baseline $t=0.9618$, proposed $t=0.9706$), accuracy increases from 0.6216 to **0.7445**. The confusion matrix shows improvement from $(TN, FP, FN, TP) = (440, 391, 671, 1304)$ to $(441, 390, 327, 1648)$ with a drop of **344** false negative. However, *Baseline + Adapter warm-up* attains ACC 0.7327, precision 0.8083, recall 0.8132, and F1 0.8107, with $(TN, FP, FN, TP) = (450, 381, 369, 1606)$. Further, we depicted heatmaps in Fig. 5 to compare the anomaly localization behavior before and after IL. The baseline PatchCore model generates widespread, low-intensity activations, suggesting limited discriminative capacity between healthy and abnormal tissue. After IL, the attention becomes significantly more focused on the lesion area, and higher saliency contrast, indicating more discriminative feature representations.

5.3 Ablation study using SWAG, MC Dropout, and Ensemble

SWAG reaches 0.89–0.90 ROC AUC in both oracle and oracle-free settings (Table 2), outperforming MC Dropout and the no-uncertainty baseline. The Ensemble variant is slightly lower than SWAG. SWAG provides robust, well-calibrated uncertainty estimates; use Ensemble when computation permits for the best overall performance, and use SWAG when efficiency is a priority, particularly in incremental and unlabeled anomaly-detection scenarios. Further, to assess the robustness of our method, we report results averaged over five independent runs with five different random seeds using the Chest_xray dataset. The bar plots in Fig. 6 show the mean performance with 95% confidence intervals for key metrics (ROC AUC, PR AUC, and F1@Youden). The narrow error bars indicate that our model exhibits low variance across runs, confirming the stability and reproducibility of the proposed approach.

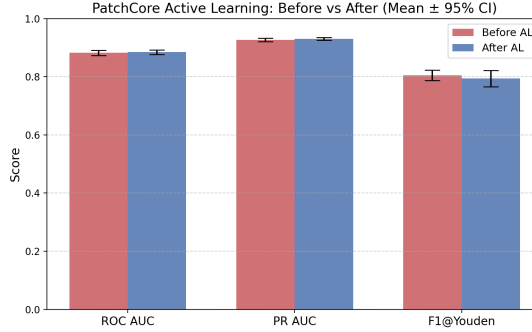


Fig. 6: Comparison (Baseline+Adapter warm up) vs. after AL on Chest_xray.

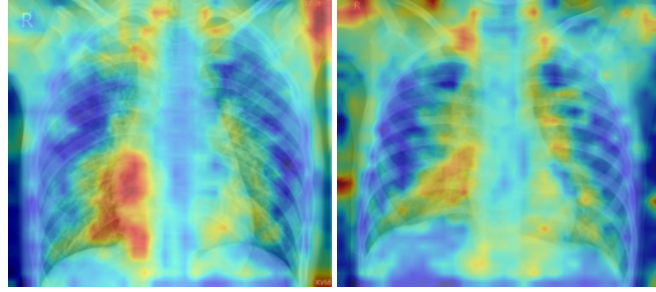


Fig. 7: Failure cases on Chest_xray, using heatmaps.

5.4 Failed Case Analysis

To illustrate failure cases of an anomaly detection model for bacterial pneumonia, we illustrated the heatmaps in Fig. 7. In the first example, the model misclassifies normal anatomical structures such as the cardiac border and diaphragm as abnormal regions, resulting in a false positive. In the second example, it fails to detect subtle and diffuse pulmonary opacities, leading to a false negative. These errors highlight the model’s sensitivity to normal intensity variations and its limited ability to recognize low-contrast infections.

5.5 Limitations

Despite strong results on standard medical-imaging benchmarks, our framework has limitations that motivate future work. Our evaluation is primarily within the medical domain; generalization to non-medical settings (e.g., industrial inspection, cybersecurity) remains untested and may stress the distance-based, uncertainty-gated admission mechanism. This is beyond the scope of this paper.

The current two-class setup may underrepresents real-world anomaly diversity (temporal shifts, contextual changes, cross-modal inconsistencies). Long-term deployment also risks domain shift: z -score gates calibrated on the seed set can drift, and SWAG’s epistemic estimates may degrade across incremental

rounds. Future extensions, such as multimodal inputs, drift-aware gate recalibration, and stronger uncertainty modeling may help us to improve adaptability and generalization beyond medical imaging. Notably, many competing methods do not fit our setting: they depend on labeled replay or oracle feedback, require periodic full-dataset retraining, or assume a static independent-and-identically-distributed (IID) stream assumptions that conflict with oracle-free incremental learning. Overall, our approach offers a practical step toward label-free, uncertainty aware incremental anomaly detection.

6 Conclusion

In this work, we presented an unsupervised and oracle-free framework for incremental anomaly learning in medical imaging. By combining SWAG-based uncertainty estimation with distance-based screening and lightweight adapter updates, the system learns what it does not know, *i.e.*, continuously refining its model of normality without supervision. By starting from a small seed of normal samples and iteratively refining the model with SWAG-guided incremental learning, our method improves detection performance without requiring any labeled anomalous data. This makes it highly practical for real-world medical imaging scenarios, where anomalies are rare, difficult to annotate, or entirely absent in training. Through extensive experiments on three publicly available medical datasets, we demonstrated that our approach consistently outperforms a baseline PatchCore system across a wide range of metrics, including ROC-AUC, PR-AUC, accuracy, precision, recall, and F1 score. Importantly, incremental learning not only improved detection sensitivity but also reduced false positives, yielding more reliable and clinically useful anomaly localization. Looking forward, our framework can be extended to other medical and industrial domains where labeled anomalies are scarce. Future work will explore integrating more advanced uncertainty quantification strategies, adapting the approach to multi-class anomaly settings, and evaluating its applicability in real-time deployment scenarios.

Acknowledgment

This work was supported by the National Science Foundation under Grant No. [#2346643](#), the U.S. Department of Defense under Award No. [#FA9550-23-1-0495](#), and the U.S. Department of Education under Grant No. P116Z240151. Any opinions, findings, conclusions or recommendations expressed in this material are those of the author(s) and do not necessarily reflect the views of the National Science Foundation, the U.S. Department of Defense, or the U.S. Department of Education.

References

1. B. Schölkopf, J. C. Platt, J. Shawe-Taylor, A. J. Smola, and R. C. Williamson, "Estimating the support of a high-dimensional distribution," *Neural Computation*, vol. 13, no. 7, pp. 1443–1471, 2001.
2. S. Ramaswamy, R. Agerri, and R. K. Srikant, "Efficient and robust clustering algorithms for large datasets," in *Proceedings of the ACM SIGKDD International Conference on Knowledge Discovery and Data Mining*, 2000.
3. T. Schlegl, P. Seeböck, S. M. Waldstein, G. Langs, and U. Schmidt-Erfurth, "f-anogan: Fast unsupervised anomaly detection with generative adversarial networks," *Medical image analysis*, vol. 54, pp. 30–44, 2019.
4. D. P. Kingma and M. Welling, "Auto-encoding variational bayes," in *Proceedings of ICLR*, 2014.
5. P. Vincent, H. Larochelle, I. Lajoie, Y. Bengio, and P. Manzagol, "Extracting and composing robust features with denoising autoencoders," in *Proceedings of the 25th International Conference on Machine Learning*, 2008.
6. I. Goodfellow, J. Pouget-Abadie, M. Mirza, B. Xu, D. Warde-Farley, S. Ozair, A. Courville, and Y. Bengio, "Generative adversarial nets," in *Proceedings of NeurIPS*, 2014.
7. K. Roth, L. Pemula, J. Zepeda, B. Scholkopf, T. Brox, and P. Gehler, "Towards total recall in industrial anomaly detection," in *Proceedings of the IEEE/CVF Conference on Computer Vision and Pattern Recognition (CVPR)*, 2022, pp. 14318–14328.
8. L. Roth, O. Dieng, J. Zepeda, and others, "Towards total recall in industrial anomaly detection," in *Proceedings of the IEEE/CVF Conference on Computer Vision and Pattern Recognition (CVPR)*, 2022, introduces PatchCore coreset memory for patch-wise AD.
9. W. J. Maddox, T. Garipov, P. Izmailov, D. Vetrov, and A. G. Wilson, "A simple baseline for bayesian uncertainty in deep learning," in *NeurIPS*, 2019.
10. J. An and S. Cho, "Variational autoencoder based anomaly detection using reconstruction probability," *Special Lecture on IE*, vol. 2, no. 1, pp. 1–18, 2015.
11. G. I. Parisi, R. Kemker, J. L. Part, C. Kanan, and S. Wermter, "Continual lifelong learning with neural networks: A review," *Neural Networks*, vol. 113, pp. 54–71, 2019.
12. S.-A. Rebuffi, A. Kolesnikov, G. Sperl, and C. H. Lampert, "icarl: Incremental classifier and representation learning," in *CVPR*, 2017, pp. 2001–2010.
13. Z. Li and D. Hoiem, "Learning without forgetting," in *ECCV*, 2016, pp. 614–629.
14. M. De Lange, R. Aljundi, M. Masana, S. Parisot, X. Jia, A. Leonardis, G. Slabaugh, and T. Tuytelaars, "A continual learning survey: Defying forgetting in classification tasks," *IEEE Transactions on Pattern Analysis and Machine Intelligence*, 2022, early versions available as arXiv:1909.08383.
15. M.-R. Bouguelia, S. Nowaczyk, K. Santosh, and A. Verikas, "Agreeing to disagree: active learning with noisy labels without crowdsourcing," *International journal of machine learning and cybernetics*, vol. 9, no. 8, pp. 1307–1319, 2018.
16. K. Santosh, "Ai-driven tools for coronavirus outbreak: need of active learning and cross-population train/test models on multitudinal/multimodal data," *Journal of medical systems*, vol. 44, no. 5, p. 93, 2020.
17. K. Santosh and S. Nakarmi, *Active learning to minimize the possible risk of future epidemics*. Springer, 2023.
18. P. Singh, R. Rizk, and K. Santosh, "Patl: Pool-based active twin learner from oracle with imitation learning for early epidemic detection," in *2025 IEEE Conference on Artificial Intelligence (CAI)*, 2025, pp. 561–566.

19. W. Yin, Z. Tan *et al.*, "An efficient replay for class-incremental learning with pre-trained models," *arXiv preprint arXiv:2408.08084*, 2024.
20. W. J. Youden, "Index for rating diagnostic tests," *Cancer*, vol. 3, no. 1, pp. 32–35, 1950.
21. D. S. Kermany, M. Goldbaum, W. Cai, C. C. Valentim, H. Liang, S. L. Baxter, A. McKown, G. Yang, X. Wu, F. Yan *et al.*, "Identifying medical diagnoses and treatable diseases by image-based deep learning," *cell*, vol. 172, no. 5, pp. 1122–1131, 2018.
22. J. P. Cohen, P. Morrison, L. Dao, K. Roth, T. Q. Duong, and M. Ghassemi, "Covid-19 image data collection: Prospective predictions are the future," *arXiv 2006.11988*, 2020. [Online]. Available: <https://github.com/ieee8023/covid-chestxray-dataset>
23. K. Santosh and S. Ghosh, "Covid-19 imaging tools: How big data is big?" *Journal of Medical Systems*, vol. 45, no. 7, p. 71, 2021.
24. M. N. Safwan, S. Rahman, M. H. Mahadi, T. M. Jabir, and I. Mobin, "Brain mri nd-5 dataset," 2024. [Online]. Available: <https://dx.doi.org/10.21227/q2vt-tf46>